Problemi teorici nello studio del plasma deconfinato con gli ioni relativistici

W.M. Alberico

Dipartimento di Fisica Teorica, Univ. of Torino and INFN, Sezione di Torino, Italy

- Introduzione
- Passato:
  1. Percolation and J/Ψ suppression
  2. Strangelets
- Presente:
  1. High density QCD
  2. Jet Quenching
- Futuro:
  1. $\bar{q}q$ bound states at $T > T_c$
  2. Unconventional statistical approaches

Introduction

The Evolving QCD Phase Transition

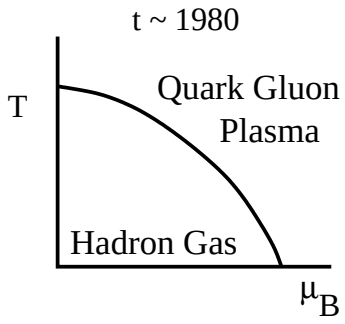

Critical Temperature 150 - 200 MeV ($\mu_B = 0$)
Critical Density 1/2-2 Baryons/Fm^3 ($T = 0$)

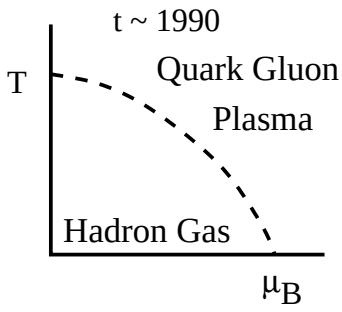

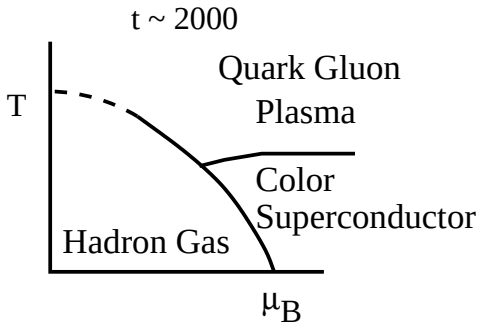

A hypothetical phase diagram for QCD is shown. The vertical axis is temperature, and the horizontal is a measure of the matter or baryon number density, the baryon number chemical potential. The solid lines indicate a first order phase transition, and the dashed line a rapid cross over. It is not known for sure whether or not the region marked cross over is or is not a true first order phase transition. There are analytic arguments for the properties of matter at high density, but numerical computation are of insufficient resolution. At high temperature and fixed baryon number density, there are both analytic arguments and numerical computations of good quality. At high density and fixed temperature, one goes into a superconducting phase, perhaps multiple phases of superconducting quark matter. At high temperature and fixed baryon number density, the degrees of freedom are those of a Quark Gluon Plasma.

Percolation and J/Ψ suppression

ref.: M. Nardi and H. Satz, Phys.Lett. B442:14-19, (1998); M. Nardi, Nucl.Phys.A681:472-475, (2001)
Percolation is a mathematical concept: regions of adjacent occupied sites or overlapping objects form clusters. When one of such clusters reaches the size of the system the system percolates.

Ordinary matter is in a colour insulating phase, although constituent partons are colored. In QGP quarks and gluons are almost free. The transition hadrons-QGP can be viewed as the onset of the colour conductivity, similar to spontaneous magnetization of ferromagnets below Curie temperature.

In a high energy nucleus-nucleus collision, many partons are liberated, as a consequence of the interactions between nucleons. Each parton of transverse momentum k_T has an effective transverse size $r \simeq k_T^{-1}$. In a nucleus-nucleus collision many such partons are produced and they overlap in the transverse plane. When their density reaches the percolation point, deconfinement sets in.

Calculate the average cluster density n_{cl} and the average cluster size S_{cl} as a function of the overall density $n = N/S_{\rm tot} = N/\pi R^2$: The point where S_{cl} has the fastest increase defines the percolation density.

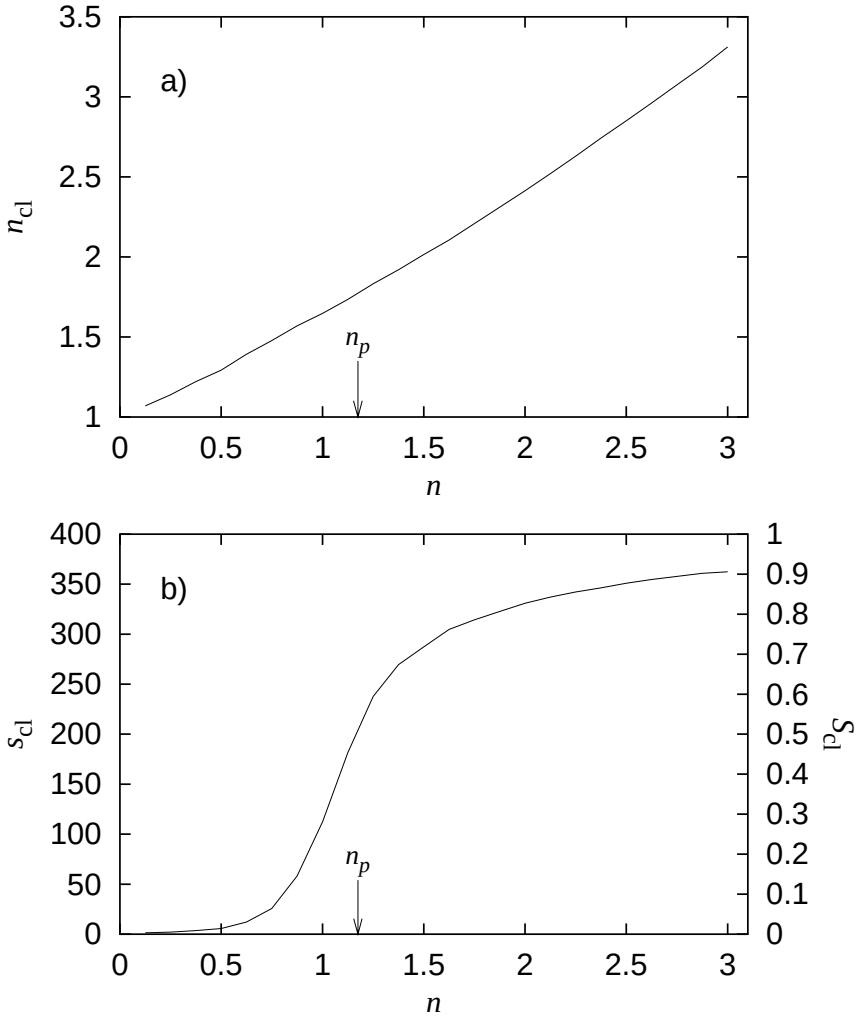

Fig. 1 – The cluster density and cluster size as function of the overall density n. $R = 5$ fm and $r = 0.25$ fm.

With $r_T = 0.27$ fm, in the Pb-Pb system, the percolation density is reached for $b \simeq 8.5$ fm: this is the impact parameter at which, experimentally, the onset of anomalous suppression is observed.

Charmonium suppression

ψ' and χ melt essentially at deconfinement while J/ψ requires a higher temperature $T(J/\psi) \simeq 1.2\, T_c$, or a higher energy density.

It is known that 40% of the observed J/ψ come from ψ' and χ decays (8% and 32% respectively) and only 60% are directly produced. Then the effective J/ψ survival probability $S^{exp}_{J/\psi}$ is a weighted average over the three charmonium components:

$$S^{exp}_{J/\psi} = 0.6\, S^{dir}_{J/\psi} + 0.32\, S_\chi + 0.08\, S_{\psi'} \qquad (1)$$

It follows a two-step pattern in the experimental J/ψ suppression: the first drop at the onset of deconfinement (ψ' and χ melt) and a second one for the suppression of the direct J/ψ component.

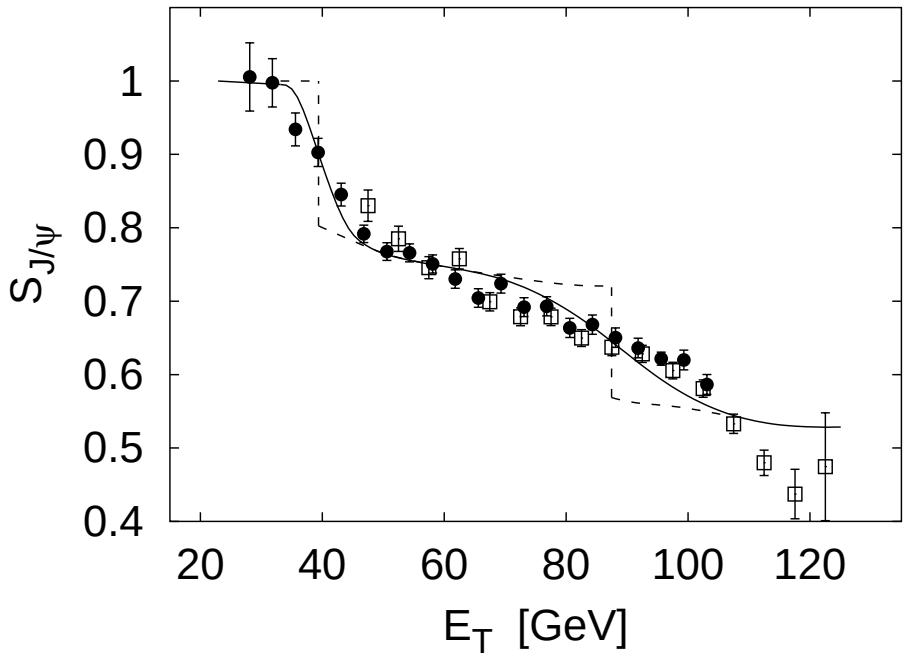

Fig. 2 – The J/ψ survival probability as function of the measured transverse energy E_T for Pb-Pb collisions at SPS energy. The dashed line corresponds to the theoretical results with fixed $E_T - b$ correlation, the solid lined includes the realistic $E_T - b$ smearing. The circles and the squares show, respectively, the 1996 and 1998 experimental results.

Strangelets

ref.: W.M.Alberico, A.Drago and C.Ratti, Nucl. Phys.**A706**:143-162, (2002)

⋆ Hypernuclear and/or strange quark matter can be realized in central relativistic heavy ion collisions, either in the form of multi-hypernuclear objects or of strange multiquark droplets. Strange matter is also interesting as a component of astrophysical objects.

⋆ Strangelets would be unambiguous signature of a pre-existing deconfined, strangeness rich state of QGP

⋆ Properties and stability of strangelets are discussed within:

1) MIT bag model (Fermi gas stabilized by vacuum pressure B), also including $\mathcal{O}(\alpha_s)$ corrections.

2) CDM, in two different versions.

3) NJL model.

⋆ The minimum energy per baryon number in homogeneous quark matter made up of u, d and s quarks, with fixed strange fraction is discussed (no β equilibrium is imposed).

⋆ Main conclusion is that stability of strangelets is model dependent. Similar investigations put in evidence the relevance of reliable effective quark models, which can be employed to study specific properties of the confined/deconfined quark matter.

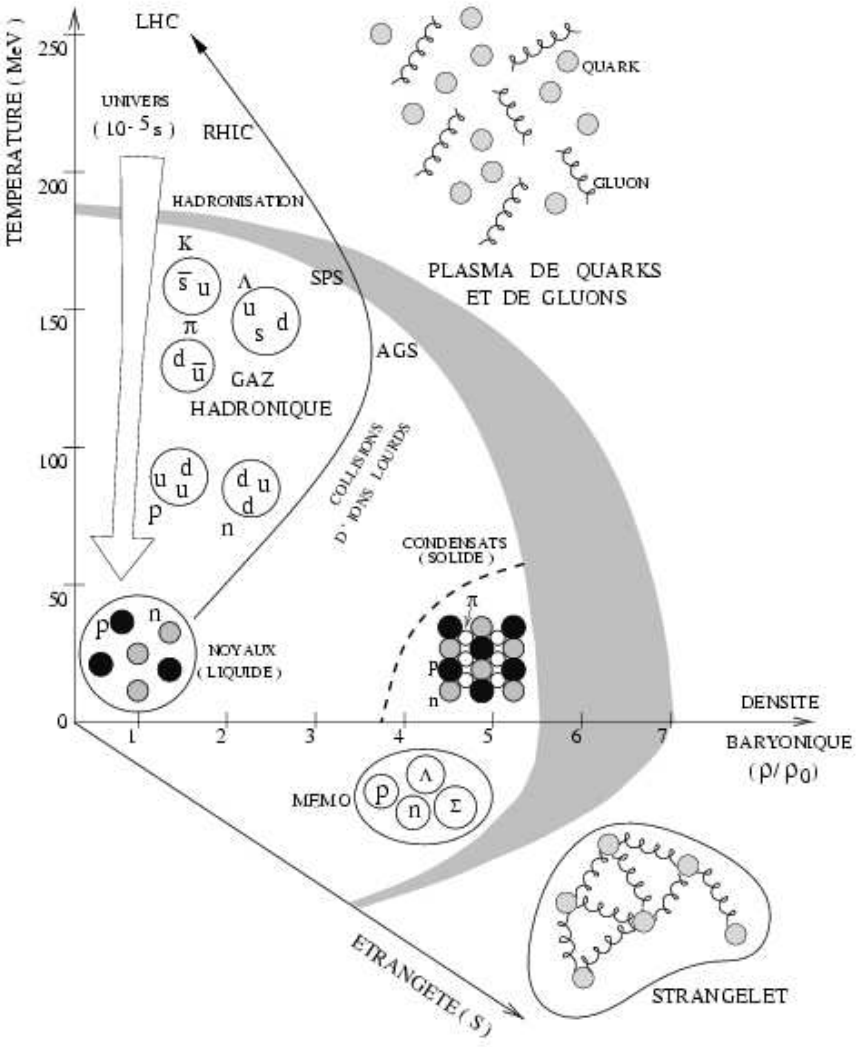

Fig. 3 – Phase diagram in the ρ, ρ_s, T space.

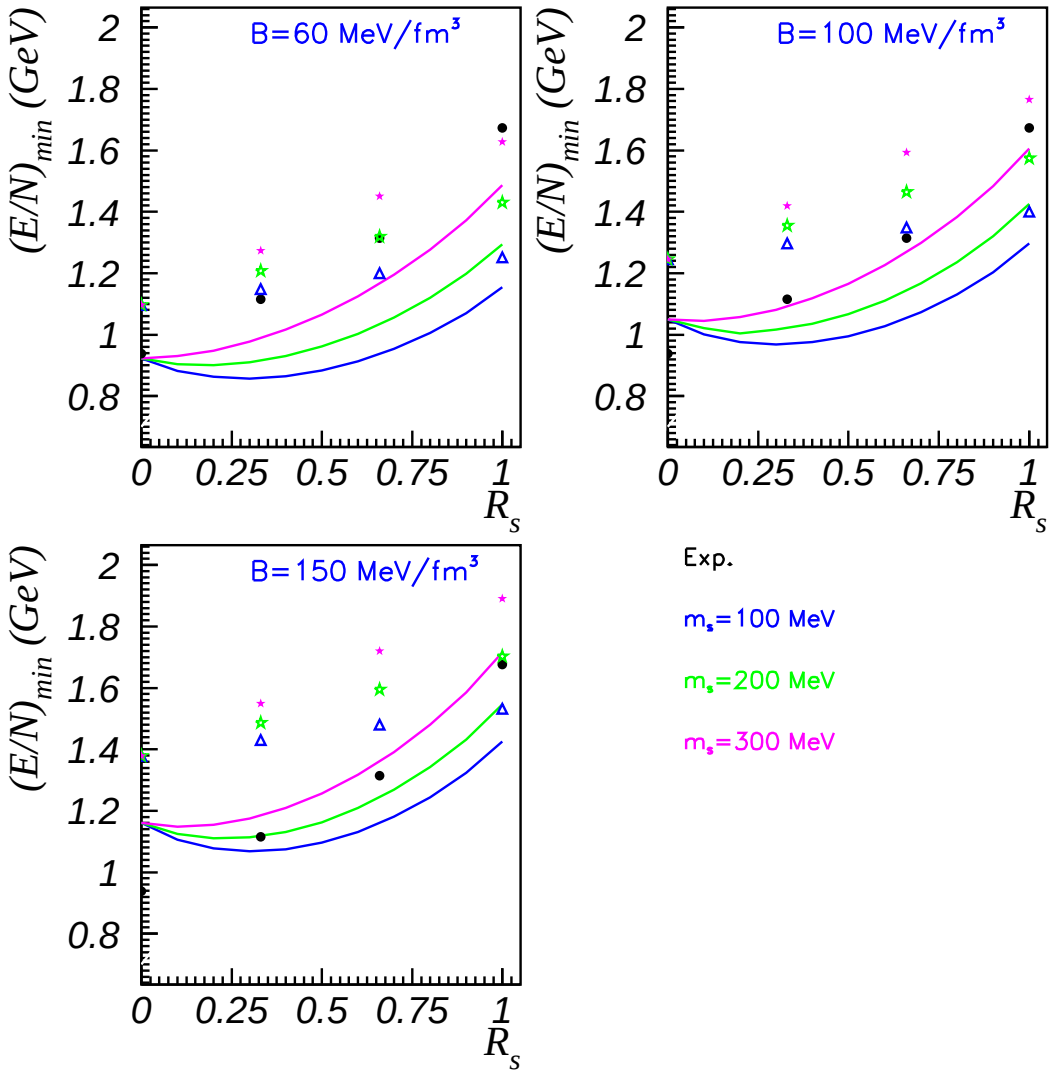

Fig. 4 – Minimal energy per baryon versus R_s in the MIT bag model without gluons, for three different values of B and three different masses of the strange quark. Full circles: experimental masses. Stars and triangles: theoretical masses evaluated according to DeGrand *et al.* PR D12 (1975) 2060.

High density QCD

ref.: D. Kharzeev and M. Nardi, Phys. Lett.**507** (2001) 121; D. Kharzeev, E. Levin and M. Nardi, arXiv: hep-ph/0111315

At RHIC the multiplicity in nuclear collisions has two components: "soft", which is proportional to the number of participants N_{part}, and "hard", which is proportional to the number of binary collisions N_{coll}:

$$\frac{dn}{d\eta} = (1-x)\; n_{pp} \frac{\langle N_{part} \rangle}{2} + x\; n_{pp}\, \langle N_{coll} \rangle\,. \qquad (2)$$

(x is fraction of the multiplicity n_{pp} measured in pp collisions per unit of (pseudo)rapidity).

Using Eq.(2), one finds that at $\sqrt{s} = 56$ GeV the fraction $F \simeq 22\%$ of the produced particles results from hard processes, while at $\sqrt{s} = 130$ GeV this fraction increases to $F \simeq 37\%$; F is defined as:

$$F = \frac{x\; n_{pp}\; N_{coll}}{dn/d\eta}. \qquad (3)$$

High density QCD and hadron production: the saturation approach

Basic ideas of saturation.

Consider a nucleus boosted to a large momentum (Lorentz–contracted), and partons "live" on a thin sheet in the transverse area π/Q^2 determined, by uncertainty principle, by its transverse momentum Q. They interact coherently with a projectile parton. The density of (target) partons in the transverse plane is:

$$\rho_A \simeq \frac{xG_A(x,Q^2)}{\pi R_A^2} \sim A^{1/3} \tag{4}$$

The cross section of the probe-parton interaction is:

$$\sigma \sim \frac{\alpha_s(Q^2)\pi}{Q^2}$$

Two regimes:

1. $\sigma\rho_A << 1$ dilute system, incoherent interactions, perturbative QCD
2. $\sigma\rho_A >> 1$ dense system, coherent interactions, collective effects.

The border between the two regimes defines the **saturation scale**, the critical value of the momentum transfer Q_s at which the parton system starts to look

dense to the probe:

$$\sigma \rho_A \simeq \frac{\alpha_s}{Q_s^2} \frac{x G_A(s, Q_s^2)}{\pi R_A^2} \sim 1 \tag{5}$$

Namely

$$Q_s^2 \sim \alpha_s(Q_s^2) \ \frac{N_A}{R_A^2} \sim A^{1/3}, \tag{6}$$

where N_A is the number of participating (and produced) partons (gluons)

$$N_A \sim \frac{1}{\alpha_s(Q^2)} \ Q^2 R_A^2 \ \sim A, \tag{7}$$

Formula (6) can be reproduced by more sophisticated methods:

$$Q_s^2 = \frac{8\pi^2 N_c}{N_c^2 - 1} \ \alpha_s(Q_s^2) \ xG(x, Q_s^2) \ \frac{\rho_{part}}{2}, \tag{8}$$

where $N_c = 3$ is the number of colors, $xG(x, Q_s^2)$ is the gluon structure function of the nucleon, and ρ_{part} is the density of participants in the transverse plane (divided by 2 to get the density of those nucleons in a single nucleus which will participate in the collision at a given impact parameter).

For a central $Au - Au$ collision at $\sqrt{s} = 130$ GeV, eq.(8) can be solved by iterations; a self–consistent solution can be found at $Q_s^2 \simeq 2$ GeV^2 if we use $xG(x, Q_s^2) \simeq 2$ at $x \simeq 2Q_s/\sqrt{s} \simeq 0.02$, with $\alpha_s(Q_s^2) \simeq 0.6$.

This can be used in the centrality dependence:

$$\frac{dN}{d\eta} = c\ N_{part}\ xG(x, Q_s^2). \tag{9}$$

where c is the *parton liberation* coefficient. One obtains good agreement with the data if $c = 1.23 \pm 0.20$.

This number appears to be close to unity, which implies a direct correspondence between the number of the partons in the initial and final states. It compares well with lattice calculation.

By assuming that the evolution of G is governed by the DGLAP equation

$$xG(x, Q_s^2) \sim \ln\left(\frac{Q_s^2}{\Lambda_{QCD}^2}\right). \tag{10}$$

one can evaluate the centrality dependence to be:

$$\frac{2}{N_{part}}\ \frac{dn}{d\eta} \simeq 0.82\ \ln\left(\frac{Q_s^2}{\Lambda_{QCD}^2}\right). \tag{11}$$

The results of these calculations in the saturation scenario are in good agreement with experiment (and also with the conventional eikonal approach).

Saturation is observed in the HERA data on deep inelastic scattering, with a saturation scale dependent on energy:

$$Q_s^2 \propto (\sqrt{s})^{\lambda}, \qquad \lambda \simeq 0.25 \div 0.3. \tag{12}$$

Then it is possible to predict $dN/d\eta$ at different energies:

$$\frac{\frac{dN}{d\eta}(\sqrt{s} = 200\,\mathrm{GeV})}{\frac{dN}{d\eta}(\sqrt{s} = 130\,\mathrm{GeV})} \simeq \left(\frac{Q_s^2(200)}{Q_s^2(130)} \right) \simeq 1.10 \div 1.14 \tag{13}$$

The last value has been confirmed by RHIC.

In the same framework predictions have been done for hadron production at energy $\sqrt{s} = 22$ GeV, not far from the highest SPS energy of $\sqrt{s} = 17$ GeV: *a priori* there is no solid reason to expect the saturation scenario to work at low energies. The data should allow to choose between two possibilities:

1) the onset of saturation occurs somewhere in the RHIC energy range, below $\sqrt{s} = 130$ GeV but above $\sqrt{s} = 17$ GeV; the mechanisms of multi–particle production at RHIC and SPS energies are thus totally different;

2) saturation sets in central heavy ion collisions already around the highest SPS energy. This would have important implications for the interpretation of the SPS results.

The formula for the energy dependence of charged multiplicity in central $Au - Au$ collisions reads:

$$\left\langle \frac{2}{N_{part}} \frac{dN_{ch}}{d\eta} \right\rangle_{\eta<1} \approx 0.87 \left(\frac{\sqrt{s}\ (\mathrm{GeV})}{130} \right)^{0.25} \times \times \left[3.93 + 0.25\ \ln \left(\frac{\sqrt{s}\ (\mathrm{GeV})}{130} \right) \right]. \qquad (14)$$

At $\sqrt{s} = 130$ GeV, one gets from Eq.(14) $2/N_{part}\ dN_{ch}/d\eta\ |_{\eta<1} = 3.42 \pm 0.15$, to be compared to the average experimental value of 3.37 ± 0.12 (PHOBOS,Phenix,Star,Brahms).

At $\sqrt{s} = 200$ GeV, one gets 3.91 ± 0.15, to be compared to the PHOBOS value of 3.78 ± 0.25.

At $\sqrt{s} = 56$ GeV, one gets 2.62 ± 0.15, to be compared to (PHOBOS) 2.47 ± 0.25.

Formula (14), when extrapolated to very high energies, predicts for the LHC energy a value substantially smaller than found in other approaches:

$$\left\langle \frac{2}{N_{part}} \frac{dN_{ch}}{d\eta} \right\rangle_{\eta<1} = 10.8 \pm 0.5; \quad \sqrt{s} = 5500\ \mathrm{GeV}, \qquad (15)$$

corresponding only to a factor of 2.8 increase in multiplicity between RHIC energy of $\sqrt{s} = 200$ GeV and LHC energy of $\sqrt{s} = 5500$ GeV.

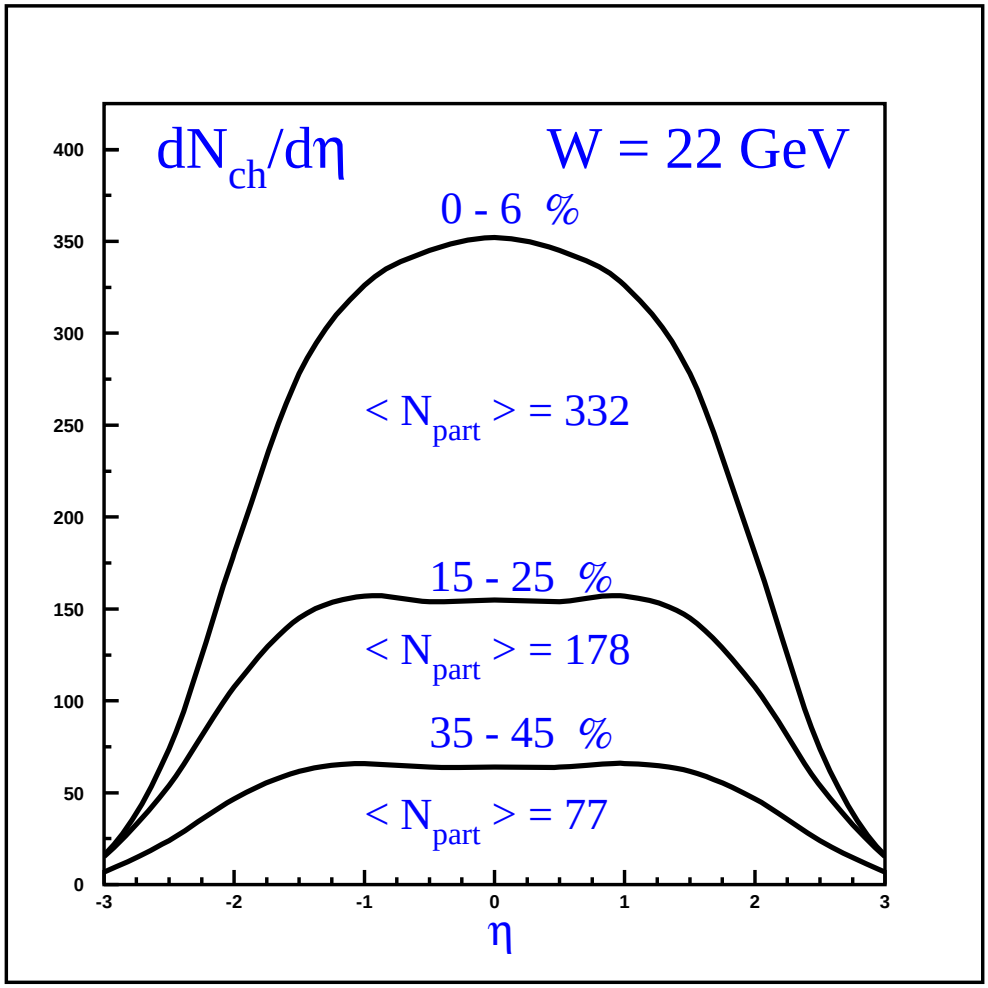

Fig. 5 – Pseudo–rapidity distribution of the charged multiplicity per participant pair in different centrality cuts at $\sqrt{s} = 22$ A GeV.

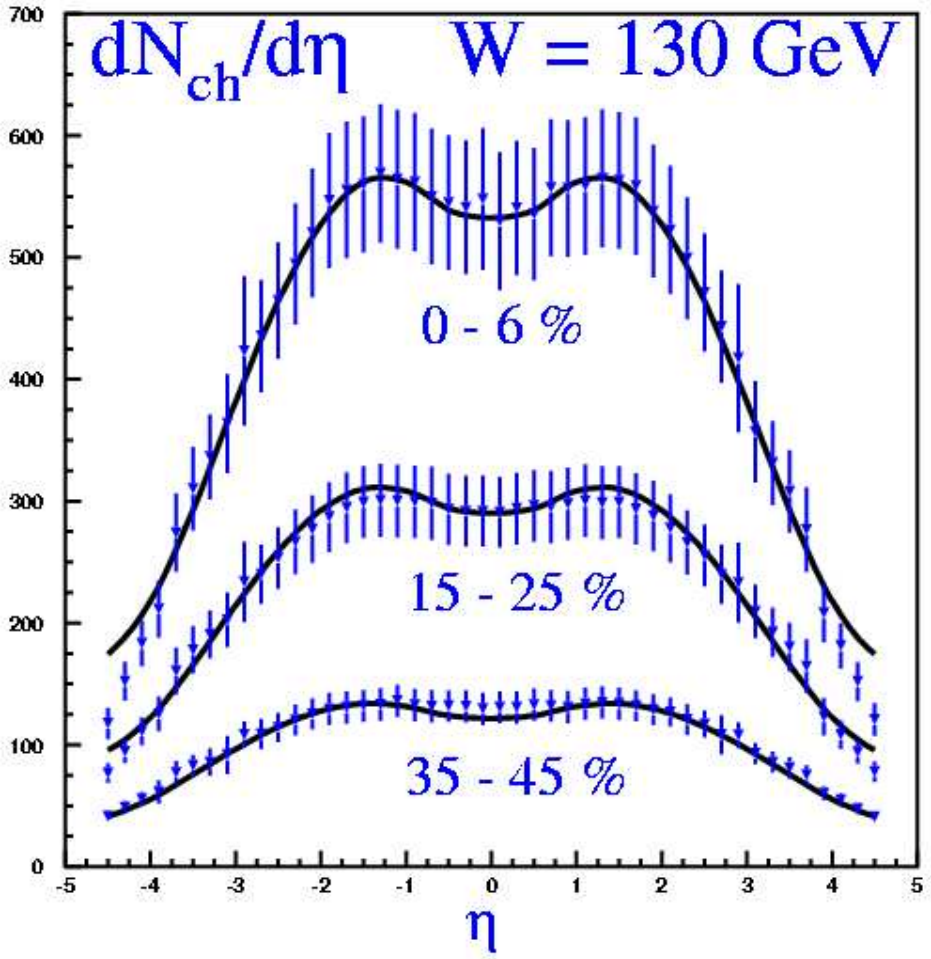

Fig. 6 – Pseudo–rapidity distribution of the charged multiplicity per participant pair in different centrality cuts at $\sqrt{s} = 130$ A GeV. Data from PHOBOS experiment.

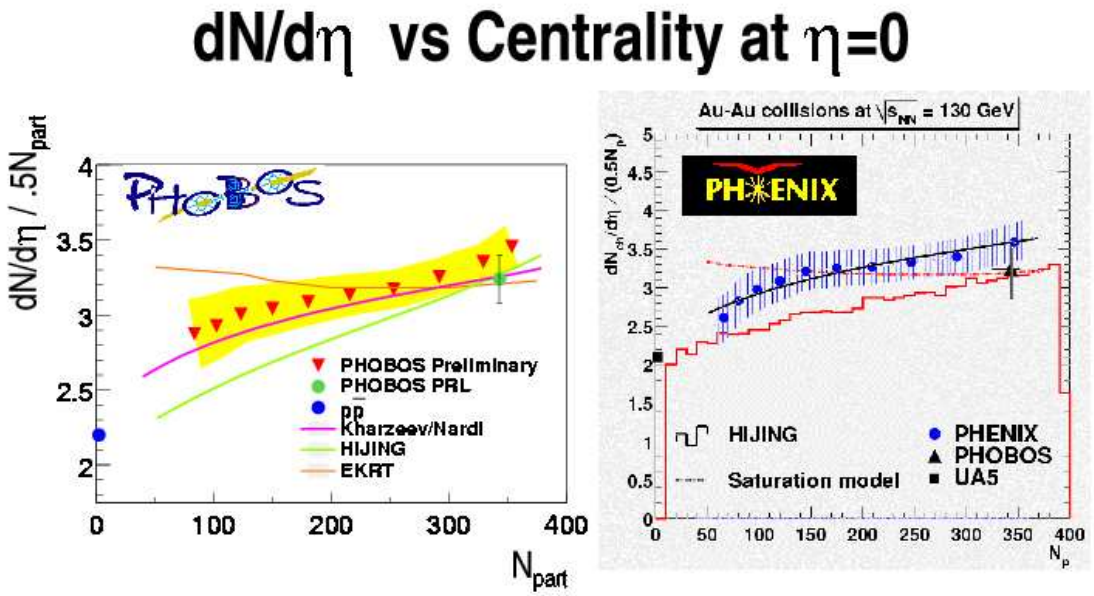

Fig. 7 – The Color Glass Condensate description of the participant dependence of the multiplicity of produced particles. Other attempts such as HIJING, or the so called saturation model of Eskola-Kajantie-Ruuskanen-Tuominen are also shown.

Jet quenching

ref.: R. Baier, Nucl. Phys. A715: 209c-218c (2003)

In August 1982 J. D. Bjorken published a preprint on "Energy Loss of Energetic Partons in Quark-Gluon Plasma: Possible Extinction of High $p_\perp$ Jets in Hadron-Hadron Collisions", in which he discussed that high energy quarks and gluons propagating through quark-gluon plasma (QGP) suffer differential energy loss, and where he further pointed out that as an interesting signature events may be observed in which the hard collisions may occur such that one jet is escaping without absorption and the other is fully absorbed.

Due to multiple (inelastic) scatterings and induced gluon radiation high momentum jets and leading large $p_\perp$ hadrons become depleted, quenched or may even become extinct. It has been shown that a genuine pQCD process is responsible for the dominant loss: after the gluon is radiated off the energetic parton it suffers multiple scatterings in the medium.

Quenching of leading hadron spectra in media

The yield of inclusive large $p_\perp$ hadrons in $A-A$ collisions is essentially modified due to the radiative medium induced energy loss, leading to significant jet quenching, i.e. to a shift of the leading particle/pion spectrum

$$\frac{d\sigma^{\rm medium}(p_\perp)}{dp_\perp^2} \simeq \frac{d\sigma^{\rm vacuum}(p_\perp + S(p_\perp))}{dp_\perp^2}\,, \qquad (16)$$

where $S(p_\perp)$ is the medium induced shift. Comparison with experiment not yet firmly established.

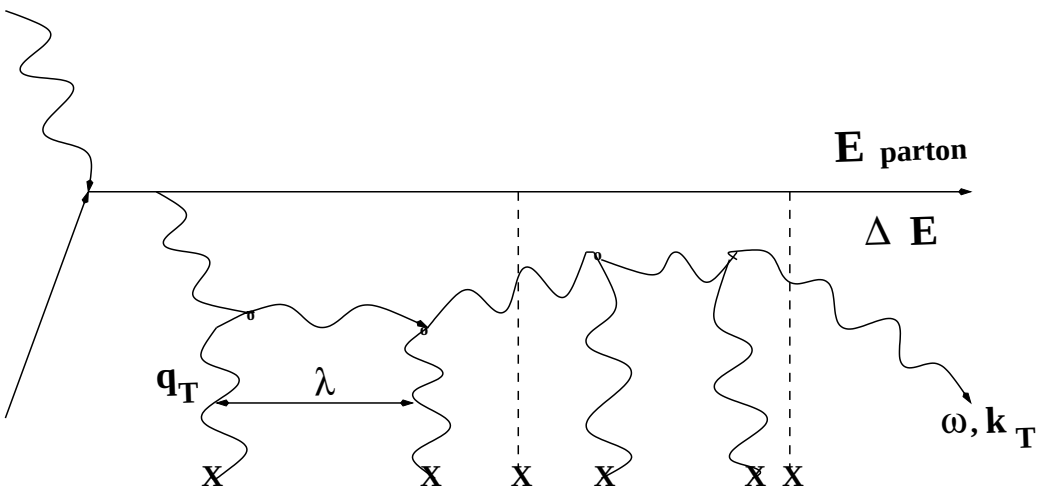

Fig. 8 – Typical gluon radiation diagram

$\bar{q}q$ bound states at $T > T_c$

ref.: JP Blaizot and E. Iancu, hep-ph/0303185
E. Shuryak, hep-ph/0312227
W.M. Alberico, A. Beraudo, A. Molinari... work in progress

i) Data from RHIC indicate robust collective flows, well described by hydrodynamics with expected equation of State. The transport properties turned out to be unexpected, with very small viscosity.

ii) Physics of highly excited matter produced in heavy ion collisions at $T_c < T < 4T_c$ is different from weakly coupled quark-gluon plasma because of relatively strong coupling generating bound states of quasi-particles.

iii) Hard Thermal Loop (HTL) expansion and related developments provide quantitative evaluation of gluons and quark masses at high temperature.

iv) The evolution in the structure of quark-antiquark bound states in going down from the so-called "zero binding points" (T_{zb}) to the QCD critical temperatures can produce interesting properties of the produced mesons. $\rightarrow$ May be interesting for the forthcoming NA60?

Unconventional Statistical approaches

ref.: W.M. Alberico, A. Lavagno and P. Quarati, Eur. Phys. J. **C12** (2000) 499; A. Lavagno, Physica **A 305** (2002) 238; A. Lavagno, Phys. Lett. **A301** (2002) 13.

Non–conventional statistical effects (due to the presence of long range forces, memory effects, correlations and fluctuations) can be relevant in the interpretation of the experimental observables in relativistic heavy-ions collisions. Transverse mass spectrum, transverse momentum fluctuations and rapidity spectra are analysed in the framework of the non-extensive statistical mechanics.

Most of the theoretical analyses related to observables in relativistic heavy-ion collisions involve (implicitly or explicitly) the validity of the standard Boltzmann-Gibbs statistical mechanics. In particular, if the thermal equilibrium is achieved, the Maxwell-Boltzmann (MB) distribution (Fermi-Dirac or Bose-Einstein distribution if quantum statistical effects are not negligible) is assumed to hold. When the system approaches equilibrium, the phase–space distribution should be derived as a stationary state of the dynamical kinetic evolution equation.

In the absence of non–Markovian memory effects, long–range interactions and local correlations, the MB

distribution is obtained as a steady state solution of the kinetic Boltzmann equation. Because of the extreme conditions of density and temperature in ultrarelativistic heavy ion collisions, memory effects and long–range color interactions can give rise to the presence of non–Markovian processes in the kinetic equation affecting the thermalization process toward equilibrium as well as the standard equilibrium distribution.

Generalized non–extensive statistics

The Tsallis generalized thermostatistics is based upon the following generalization of the entropy

$$S_q = \frac{1}{q-1} \sum_{i=1}^{W} p_i \left(1 - p_i^{q-1}\right) , \qquad (17)$$

where p_i is the probability of a given microstate among W different ones and q is a fixed real parameter. The new entropy has the usual properties of positivity, equiprobability, concavity and irreversibility, preserves the whole mathematical structure of thermodynamics and reduces to the conventional Boltzmann–Gibbs entropy $S = -\sum_i p_i \log p_i$ in the limit $q \to 1$.

The single particle distribution function is obtained through the usual procedure of maximizing the Tsallis entropy under the constraints of keeping constant the average internal energy and the average number of

particles. For a dilute gas of particles and/or for $q \approx 1$ values, the average occupational number can be written in a simple analytical form

$$\langle n_i \rangle_q = \frac{1}{[1 + (q-1)\beta(E_i - \mu)]^{1/(q-1)} \pm 1} \,, \qquad (18)$$

where the $+$ sign is for fermions, the $-$ for bosons and $\beta = 1/T$. In the limit $q \to 1$ (extensive statistics), one recovers the conventional Fermi–Dirac and Bose–Einstein distribution.

When the entropic q parameter is smaller than 1, the distribution (18) has a natural high energy cut–off: $E_i \leq 1/[\beta(1-q)] + \mu$, which implies that the energy tail is depleted; when q is greater than 1, the cut–off is absent and the energy tail of the particle distribution (for fermions and bosons) is enhanced. Hence the nonextensive statistics entails a sensible difference of the particle distribution shape in the high energy region with respect to the standard statistics.

Transverse mass spectrum and momentum fluctuations

For small deviations from standard statistics $(q - 1 \approx 0)$; then at first order in $(q-1)$ the transverse mass spectrum can be written as

$$\frac{dN}{m_\perp dm_\perp} = C\, m_\perp \left\{ K_1(z) + \frac{(q-1)}{8} z^2 \, [3\, K_1(z) + K_3(z)] \right\} \,, \qquad (19)$$

where K_i are the modified Bessel function at the i-order.

The above equation is able to reproduce very well the transverse momentum distribution of hadrons produced in S+S collisions (NA35 data) providing we take $q = 1.038$. Furthermore, it is easy to see that at first order in $(q-1)$ from Eq.(19), the generalized slope parameter takes the following form:

$$T_q = T + (q-1)\, m_\perp \ . \tag{20}$$

Hence nonextensive statistics predicts, in a purely thermal source, a generalized q–blue shift factor at high $m_\perp$; moreover this shift factor is not constant but increases (if $q > 1$) with $m_\perp = \sqrt{m^2 + p_\perp^2}$, where m is the mass of the detected particle. Such a behavior has been observed in the experimental NA44 results.

Another observable very sensitive to non–conventional statistical effects are the transverse momentum fluctuations, which however are more difficult to unambiguously extract from the experimental data.

Anomalous diffusion in rapidity spectra

An important observable in relativistic heavy-ion collisions is the rapidity distribution of the detected particles. In particular, there is experimental and theoretical evidence that the broad rapidity distribution of net proton yield $(p-\overline{p})$ in central heavy-ion collisions at SPS energies could be a signal of non-equilibrium properties of the system. This broad rapidity shape can be well reproduced in the framework of a non-linear relativistic Fokker-Planck dynamics which incorporates non-extensive statistics and anomalous diffusion.

A class of anomalous diffusions are currently described through the non-linear Fokker-Planck equation (NLFPE)

$$\frac{\partial}{\partial t}[f(y,t)]^{\mu} = \frac{\partial}{\partial y}\left[J(y)[f(y,t)]^{\mu} + D\frac{\partial}{\partial y}[f(y,t)]^{\nu}\right] , \tag{21}$$

where D and J are the diffusion and drift coefficients, respectively. Tsallis and Bukman have shown that, for linear drift, the time dependent solution of the above equation is a Tsallis-like distribution with $q = 1 + \mu - \nu$. The norm of the distribution is conserved at all times only if $\mu = 1$, therefore we will limit the discussion to the case $\nu = 2 - q$.

Imposing the validity of the Einstein relation for Brownian particles, one can generalize to the relativistic case the standard expressions of diffusion and drift

coefficients:

$$D = \alpha\, T\ , \qquad J(y) = \alpha\, m_\perp \sinh(y) \equiv \alpha\, p_\parallel\ , \tag{22}$$

where $p_\parallel$ is the longitudinal momentum and α is a common constant. The stationary solution of the NLFPE (21) with $\nu = 2 - q$ is a Tsallis-like distribution with the relativistic energy $E = m_\perp \cosh(y)$:

$$f_q(y, m_\perp) = \left\{1 - (1-q)\,\beta\, m_\perp \cosh(y)\right\}^{1/(1-q)}\ . \tag{23}$$

Basic assumption of the analysis is that the rapidity distribution is not appreciably influenced by transverse dynamics, which is considered in thermal equilibrium. The time dependent rapidity distribution turns out to be:

$$\frac{dN}{dy}(y,t) = c \int_m^\infty m_\perp^2\ \cosh(y)\, f_q(y, m_\perp, t)\, dm_\perp\ , \tag{24}$$

where c is the normalization constant fixed by the total number of the particles. The calculated rapidity spectra will ultimately depend on the nonextensive parameter q only, since there exists only one "interaction time" $\tau = \alpha t$ which reproduces the experimental distribution.

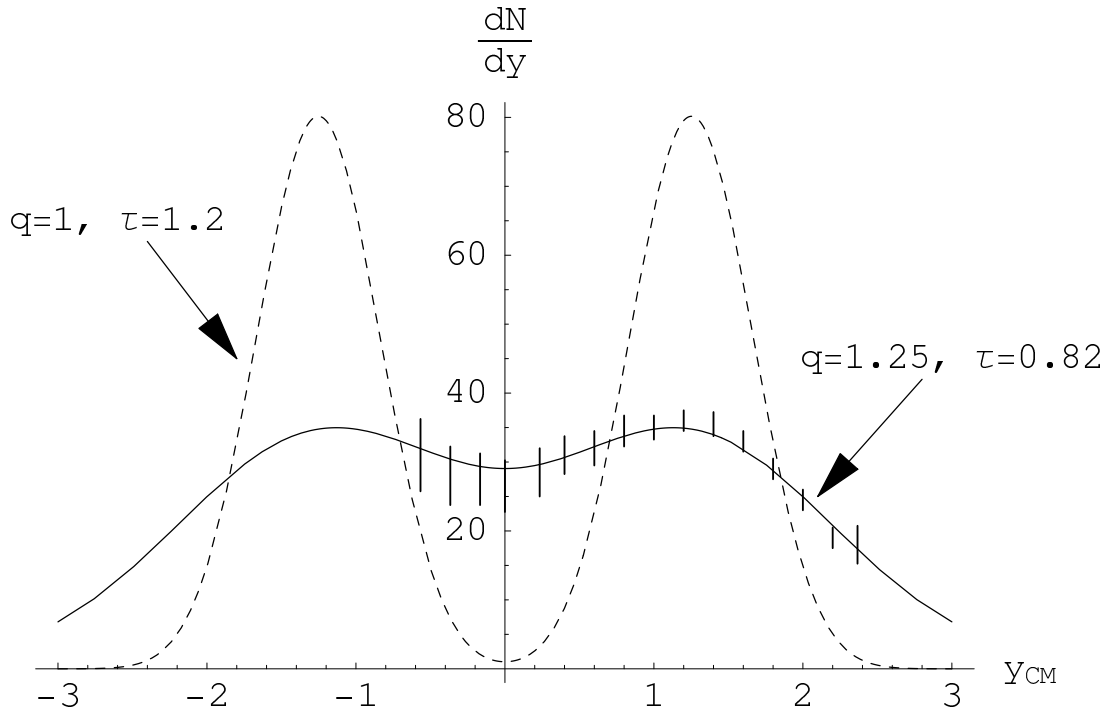

Fig. 9 – Rapidity spectra for net proton production $(p - \overline{p})$ in central Pb+Pb collisions at 158A GeV/c (grey circles are NA49 data reflected about $y_{cm} = 0$). Full line corresponds to the results obtained by using a non-linear evolution equation ($q = 1.25$), dashed line corresponds to the linear case ($q = 1$).